Triple Oxygen Isotopic Compositions of Ocean Water from the Mariana Trench

Ying Lin, Nanping Wu, Kaiwen Ta, Amaelle Landais, Xiaotong Peng

Triple oxygen isotopic compositions of ocean water from Mariana Trench

Journal:	*ACS Earth and Space Chemistry*
Manuscript ID	sp-2021-001872.R3
Manuscript Type:	Article
Date Submitted by the Author:	n/a
Complete List of Authors:	Lin, Ying; Institute of Deep-sea Science and Engineering, Chinese Academy of Sciences, Luhuitou Road No. 28, Sanya, Hainan 572000, China, Wu, Nanping; Chinese Academy of Sciences, Ta, Kaiwen; Sanya Institute of Deep-sea Science and Engineering Chinese Academy of Sciences Landais, Amaelle; LSCE Peng, Xiaotong; Institute of Deep-sea Science and Engineering, Chinese Academy of Sciences , Deep Sea Research Department

Triple oxygen isotopic compositions of ocean water from Mariana Trench

Ying Lin[1,2,*], Nanping Wu[1]*, Kaiwen Ta[1], Amaelle Landais[3], Xiaotong Peng[1]

[1]Institute of Deep Sea Science and Engineering, Chinese Academy of Sciences, Sanya, Hainan, China 572000

[2]Department of Earth and Planetary Sciences, University of California, Riverside, CA 92521

[3]Laboratoire des Sciences du Climat et l'Environnement, UMR 8212, IPSL, CEA/CNRS/UVSQ, 91190 Gif sur Yvette, France

*Ying Lin, Nanping Wu

Email: yinglin@ucr.edu, wunp@idsse.ac.cn

Keywords: Mariana Trench, Triple Oxygen Isotopes, Isotope Thermometry, Ocean Isotope Mass Balance Model, Gross Oxygen Productivity

ABSTRACT:

High precision triple oxygen isotope data on 40 water samples (5 to 10,923 m depth) collected at the Challenger Deep of Mariana Trench are reported in this study. The analyses at Laboratoire des Sciences du Climat et l'Environnement (LSCE) yield mean isotope values $\delta^{18}O$ = –0.084 ± 0.224 ‰, $\delta^{17}O$ = –0.061 ± 0.117 ‰, and ^{17}O-excess = –17 ± 5 per meg, with standard deviations reported at 1σ. The range of $\delta^{18}O$ (–0.480 to 0.544 ‰) falls within records of Global Seawater Oxygen-18 Database at Mariana Trench. Average ^{17}O-excess value at Mariana Trench is more negative than the average ^{17}O-excess value of –5 ± 4 (1σ) per meg in the only prior dataset including deep ocean samples. The slope (λ) of the three-isotope-plot of Mariana Trench water is 0.521 ± 0.003 (1σ), lower than λ of 0.528± 0.001 (1σ) for ocean water in the prior study. The new dataset matches the prediction of ocean isotope mass balance model, suggesting it may represent a more appropriate ocean endmember for triple oxygen isotope thermometry. The ^{17}O-excess of ocean water with respect to VSMOW is recognized to be a necessary correction in quantifying gross oxygen productivity of euphotic regions and relative humidity of moisture source regions.

1. INTRODUCTION

Oxygen isotopic compositions are reported in delta notation[1]:

$$\delta^x O = \left(\frac{^xO/^{16}O_{sample}}{^xO/^{16}O_{standard}} - 1\right) \times 1000 \qquad \text{Eq.(1)}$$

where x is 17 or 18 and δ is reported in permil (‰).

Small ^{17}O anomalies arise from fundamental differences between individual mass dependent fractionation mechanisms (equilibrium vs. kinetic). The basic theory for mass-dependent triple oxygen isotope fractionation was established early on[2-3], however its application relies on high precision isotope analytical techniques, which are recently available for minerals and water[4]. Novel research related to the meteoric water cycle has been inspired by resolving differences between equilibrium and kinetic isotope effects for water[5-6], to depict continental moisture recycling[7], snow formation[8, 9], and reconstruct paleoenvironments[10, 11]. The ^{17}O-excess relevant to studies on the hydrological cycle is calculated by Eq.(2), with a reference slope λ value of 0.528[12-13], and expressed in per meg:

$$^{17}O\text{ - }excess = [\ln\left(1 + \delta^{17}O/1000\right) - \lambda \ln\left(1 + \delta^{18}O/1000\right)] \times 10^{6} \qquad \text{Eq. (2)}$$

To be consistent with “permil” for delta notation where “milli” is Latin origin meaning one thousand, we use “per meg” for ^{17}O-excess in this study since “mega” is Greek origin meaning one million. However, “ppm” is often also used in the literature.

Conventional oxygen isotope thermometry, which draws on the information of equilibrium oxygen isotopic signatures ($^{18}O/^{16}O$ ratios) between minerals and water, has been applied to estimate temperatures in modern and past climates and infer glacial history[14-17]. Recently, triple oxygen isotope system ($^{18}O/^{16}O$ and $^{17}O/^{16}O$ ratios) is developed to distinguish mass dependent equilibrium and kinetic

processes by analyzing oxygen-bearing silicates, carbonates, sulfates, phosphates etc. at low *T* environments and hydrothermal altered, igneous and metamorphic rocks at high *T* environments[4]. The implementation of an extra dimension to $\delta^{18}O$ scale quantitatively constrains geological processes and accurately reconstructs paleoclimate and paleoenvironment, manifested in: a) rigorous tests of assumptions such as equilibrium in palaeothermometry; b) tests of proposed kinetic reaction mechanisms[18-19]; c) constraints of pristine oxygen isotopic composition of water, water/rock ratio, or *T* in water-rock interaction[20]; d) providing insights into diagenesis processes[21-22]; e) explanation of the secular sedimentary trends[23]; f) identification of effects of evaporation and aridity[24].

Well-constrained modern and ancient oxygen isotopic compositions of ocean water serve as an anchor for wide applications in climate sciences and Earth sciences. There's a good amount of ocean water $\delta^{18}O$ records including deep oceans[25]. However, there's a lack of triple oxygen data for ocean water, especially from the deep oceans, inhibiting the confidence in the potential applications of triple oxygen isotopes. A prior triple oxygen isotope study of seawater analyzed 38 water samples from the Atlantic Ocean, the Pacific Ocean, E. Mediterranean and northern Red Sea at variable depths (2-5196 m)[13]. In the current study, 40 water samples were collected from Mariana Trench by researchers from the Deep-sea Institute of Science and Engineering, Chinese Academy of Sciences.

2. MATERIALS AND METHODS

Two hadal cruises R/V Xiangyanghong Jiuhao (37II) and Tansuo Yihao (TS09) were carried out between June 2016 and September 2018. During the cruises, a total of 22 stations, with water depths ranging from 5 to 10923 m, were investigated from the Challenger Deep and overlying water column. Water samples were collected in Niskin bottles from the southern (stations JL115, JL120, JL122, JL144, JL146, 37II-CTD01, 37II-CTD03, 37II-CTD05), middle (stations Dive YW17, Dive YW18, Dive YW19, Dive YW20, Dive YW21, Dive YW22, Dive YW23, Dive WQ20, Dive WQ21, Dive WQ22, Dive WQ23, Dive WQ24 and TS09-CTD06) and northern (station JL150) regions of the Mariana Trench in the Western Pacific Ocean (Figure 1, Table S1). Niskin bottles (Sea-Bird, Bellevue, WA, USA) were attached to the Jiao Long Human Occupied Vehicle, Hadal landers (Wangquan and Tianya), and a CTD rosette to obtain water samples. All of the Dive samples were collected tens of centimeters above the sediment surface. Sampling depth was recorded by the Niskin bottle CTD rosette (SeaBird SBE 19plus V2 SEACAT). Water samples were filtered onboard through a 0.22 μm pore size polytetrafluoroethylene membrane (Millipore, Massachusetts, USA)[26] and stored at –20 °C immediately afterward until further processing.

Triple oxygen isotope analyses of water samples were carried out in June 2019 at the Laboratoire des Sciences du Climat et l'Environnement (LSCE), Gif sur Yvette, France. The analytical procedure of CoF_3 fluorination of water followed by the measurement of product O_2 with a ThermoScientific MAT 253 gas source

isotope ratio mass spectrometer is described in Landais et al.[27] Water samples were analyzed in duplicates. Three in-house standards were fluorinated and measured along with three international standards (VSMOW2, GISP2, SLAP2). Triple oxygen isotope values are normalized to SMOW2/SLAP2 scale (Table 2)[28]. Uncertainties for $\delta^{18}O$, $\delta^{17}O$, and ^{17}O-excess are 0.020 ‰, 0.015 ‰, and 6 per meg respectively, derived from 1σ standard deviations of replicate samples. The uncertainties derived from repeated standards are smaller.

3. RESULTS

The $\delta^{18}O$ values vary from –0.480 to 0.544 ‰, $\delta^{17}O$ values vary from –0.267 to 0.270 ‰, and ^{17}O-excess values range from –29 to –6 per meg for water samples in this study (Table 1, Figure 2). No apparent depth variations are observed except for relatively low ^{17}O-excess down to –29 per meg at 5-7 km and more variable $\delta^{18}O$ and $\delta^{17}O$ at ~11 km than at shallower depths. In the three-isotope plot, our data define a slope λ= 0.521±0.003 (1σ) (Figure 3A). In contrast, the dataset of Luz and Barkan[13] yields slopes λ= 0.521±0.010 (1σ) for 16 Pacific deep waters (500-5196 m) (Figure 3B), λ= 0.531±0.004 (1σ) for 14 Atlantic surface waters (0-2 m) (Figure 3C), and λ= 0.528±0.001 (1σ) for all samples (Figure 3D). The three-isotope plots are generated by MATLAB_R2021a, Natick, Massachusetts: The MathWorks Inc., slopes and the 1σ standard errors of linear least square fits are calculated by JMP®, Version <*16*>. SAS Institute Inc., Cary, NC, 1989–2021.

Our data fall within the range of $\delta^{18}O$ from Global Seawater Oxygen-18 Database[25, 29-30] in vicinity of our sampling locations (–0.3 to 0.87 ‰ and one sample of 2.8 ‰, Table S2).

In order to evaluate how triple oxygen isotopic compositions of water samples varied over the large depth range in this study, we binned our data into varying depth ranges (Table S3) and compared those average values to the un-binned averages. The results do not reveal an obvious depth-dependent structure to the isotopic measurements, so we applied simple average $\delta^{18}O$, $\delta^{17}O$, and ^{17}O-excess values -0.084 ± 0.224 (1σ) ‰, -0.061 ± 0.117 (1σ) ‰ and -17 ± 5 (1σ) per meg throughout this study.

The average ^{17}O-excess value of –17 ± 5 per meg from this study is more negative than –5 ± 4 (1σ) per meg from Luz and Barkan[13]. While there are potential analytical biases, we expect these to be significantly smaller than the difference in mean values reported here (discussed below). Therefore, the differences in ^{17}O-excess from this study and the prior study are likely to be environmentally meaningful in using triple oxygen isotopes as a tracer of physical processes in the ocean.

4. DISCUSSION

There are analytical challenges in water fluorination and triple oxygen isotope measurement, which may result in significant inter-laboratory offsets of

^{17}O-excess[11]. For O_2 analytes, the lower abundance of ^{17}O relative to ^{16}O and ^{18}O may result in the larger scaling of ^{17}O-excess values and this pressure baseline (PBL) effect worsens as the difference in isotope compositions between sample and reference gas increases[31]. Wostbrock et al.[32] found no PBL effect in analyzing two gases with δ^{18}O values differ by 25 ‰ at 3, 5, 10 V intensities of m/z 32, thus suggested that the artifact is instrument-specific. This PBL effect was not evaluated at LSCE. However, scale distortion should have a negligible effect on the ^{17}O-excess values of ocean water for it is close to VSMOW in isotopic composition. Potential interlaboratory difference in ^{17}O-excess may also arise from different standardization regimes. Isotope values from this study are normalized to VSMOW2/SLAP2 scale, whereas Luz and Barkan[13] chose not to normalize their isotope values to the VSMOW/SLAP scale but instead recorded a 0.4 ‰ difference between their measured and consensus values of δ^{18}O of SLAP. As potential analytical biases are small compared to the differences between this dataset and that of Luz and Barkan[13], we believe these differences represent real environmental variations. Thus we further interpret our data and discuss potential applications.

Oxygen isotope fractionation exponent, θ, is defined by Eq. (3):

$$\theta = \frac{\ln^{17}\alpha}{\ln^{18}\alpha} \qquad \text{Eq. (3)}$$

where α is the oxygen isotope fractionation factor. For liquid-vapor equilibrium, $\alpha_{\text{L-V}}$ is defined by Eq. (4):

$$^{x}\alpha_{L-V} = \frac{(^{x}O/^{16}O)_{L}}{(^{x}O/^{16}O)_{V}} \quad \text{Eq. (4)}$$

where *x* is 18 or 17.

We compare the slope (λ) of the three-isotope plot of data from this study and those from the study of Luz and Barkan[13] to the θ values characterizing distinct processes. The λ may represent multiple processes while θ represents a specific process[2] and λ is replaceable by θ for equilibrium or reproducible kinetic isotope fractionations[33].

The isotopic composition of Mariana Trench waters reflects their source waters in the surface ocean, and subsequent physical processes during water mass transport. The oxygen isotope fractionation slopes for liquid-vapor equilibrium of water at air-sea interface and water liquid-liquid self-diffusion endmembers are discussed briefly below. We demonstrate that the slope of three-isotope plot for the measured Mariana Trench waters is intermediate between those expected process endmembers.

4.1 PROCESSES AT OCEAN SURFACE

Oxygen isotope mass balance of open-ocean surface water can be described by Craig-Gordon model with recharge, discharge, and evaporation[34-37]. The air-sea interface is characterized by liquid-vapor equilibrium of water. Triple oxygen isotope exponent θ_{eq}=0.529±0.001 (1σ) was experimentally determined for liquid-vapor equilibrium of water from 11.4 to 41.5 ºC[5]. It is very close to 0.530 calculated based on quantum statistical mechanics and ~0.529 calculated based on vapor pressure isotope effects in condensed systems[38-39]. The θ_{eq} between liquid water/ice and water vapor has extremely small temperature dependence of ~4×10^{-6} K^{-1} over the range of –20 to +20 ºC[39]. Over the temperature range –25 to 40 ºC, the slope λ value that characterizes Rayleigh distillation and rainout process is 0.527-0.529[6, 12-13], slightly higher at warmer temperatures and slightly lower at cooler temperatures[27]. At a sea surface temperature of 10 ºC, the equilibrium fractionation factor $^{18}\alpha_{eq}$=1.01073[40] and θ_{eq}=0.529 translate into $\lambda=(^{17}\alpha_{eq}-1)/(^{18}\alpha_{eq}-1)$=0.528 for Rayleigh distillation[6]. Atlantic surface water sample subset from Luz and Barkan[13] exhibits a λ of 0.531±0.004 (Figure 3C), suggesting near-equilibrium exchange at Atlantic ocean surface.

4.2 PROCESSES IN OCEAN INTERIOR

Advection, molecular diffusion, and turbulent diffusion are major processes in ocean interior regulating seawater masses. Turbulent mixing in the interior of the ocean is produced by planetary Rossby waves, mesoscale eddies (generated by baroclinic instability slumping the horizontal density gradient), and internal

waves (generated by winds and tides)[41-42]. Molecular diffusion including concentration/chemical diffusion (self-diffusion for chemically identical species) and Soret diffusion can be driven by small-scale variabilities in salinities and temperatures, respectively[43-44].

Self-diffusion coefficient (*D*) of liquids is predicted by kinetic gas theory[45-47]. For self-diffusion of water, the relevant exponent θ_k has a value of 0.514 based on the ratios of self-diffusivities (Eqs.S1-2).

For vertical eddy diffusion, Fick's first law can be applied as the ocean is generally vertically stratified with large concentration gradients with depth[48]. Theoretically, kinetic isotope effect of Fick's diffusion is given by the kinetic mass-dependent fractionation law as Eq.(S3)[3]. The θ_k value of 0.516 is calculated by Eq.(S3) with atomic masses of oxygen, while θ_k=0.514 using molecular masses of water[49].

4.3 OBSERVATION AT MARIANA TRENCH

The observed λ=0.521±0.003 (1σ) for Mariana Trench waters and λ= 0.521±0.001 (1σ) for Pacific deep waters from Luz and Barkan[13] (Figure 3) imply that the interior ocean processes modify signals from the surface ocean with θ_{eq}=0.529±0.001(1σ) and is consistent with additional diffusion and its associated kinetic fractionation along the interior flow path. Other than intrinsic kinetic processes, water mass of the deep Mariana Trench is originated from upwelling of

the southern Circumpolar Deep Water[50], and kinetic isotope effect associated with diffusion process was found to be present with sea-ice formation at Antarctica[51].

While the direction of depletion in the Mariana samples is suggestive, λ=0.521 from our dataset (0.515 to 0.527, 95%CI) cannot be conclusively distinguished from the other empirical and theoretical slopes, including for the kinetic (θ_k =0.514 and/or 0.516) or equilibrium (θ_{eq}=0.529, 0.527 to 0.531 95%CI) fractionation, or the prior world ocean dataset (λ=0.528, 0.526 to 0.530 95%CI). Combining Pacific deep water subset[13] with Mariana waters, the average ^{17}O-excess is –13±8 (1σ) per meg. Combing world ocean data[13] with Mariana waters, the average ^{17}O-excess is –11±8 (1σ) per meg.

Diapycnal mixing of different water masses has been known for ocean bodies[25] and can explain the range of isotope values observed in depth profiles (Figure 2). Plotting our data and W.Pacific data from the Global Seawater Oxygen-18 Database[29] (Figure 4), we can infer the mixing of Circumpolar Deep Water (CPDW) including AABW (Antarctic Bottom Water, with δ^{18}O of ~–0.6 ‰ and salinity of ~34.65 g/kg) and AAIW (Antarctic Intermediate Water, with δ^{18}O of ~–0.3 ‰ and salinity of ~34.2 g/kg) into the Pacific Ocean originally described by Big and Rohling[25]. The apparent variability in the bottom ocean waters may have to do with higher sampling density and we may observe similar variability in the more abundantly sampled upper ocean waters.

We present the first published deep ocean profiles of the triple oxygen isotopic composition of seawater. These reveal previously unmeasured ^{17}O depletions at depth that may imply a different bulk composition of water on Earth than implied by the upper ocean and meteorological measurements to date. The novel dataset allows scientists to test underlying assumptions for the interpretation of triple oxygen isotopes in a number of applications. Specific implications for the measured values are detailed in the next section.

5. APPLICATIONS

5.1 TRIPLE OXYGEN ISOTOPE THERMOMETRY

Traditional dual oxygen isotope thermometers were calibrated at various temperature ranges for carbonates, silicates, oxides, hydroxides, phosphates, sulfates, and salts between mineral phases and between minerals and waters, based on experimental, empirical, and theoretical methods[14, 17, 52]. In the recent years, triple oxygen isotope fractionation factors between silicates, carbonates, phosphates, sulfates and water were computed theoretically and calibrated experimentally and empirically[22, 38, 53-57] and applied in triple oxygen isotope thermometers for Earth surface and low-*T* hydrothermal environments[58-59]. Our study provides isotope values of the seawater endmember for many marine mineral-water equilibrium systems.

Mineral-water equilibrium is given by Eq. (5)[22]:

$$^{17}O-excess_{mineral} = 1000[^{17}O-excess_{water} + \left(\frac{a\times10^6}{T^2} + \frac{b\times10^3}{T} + c\right)\left(0.5305 - \frac{\varepsilon}{T} - \lambda\right)] \quad \text{Eq. (5)}$$

where *a*, *b*, *c*, ε are constants and λ=0.528. The original equation uses "$\Delta'^{17}O$" terminology, however we use "^{17}O-excess" for consistency.

For silicate-seawater equilibrium, *a*=4.28, *b*=–3.5, *c*=0, ε=1.85[53]. A chert sample from Horizon Guyot, Pacific Ocean (168°52.3′W, 10°28.0′N, 1700 m water depth) has a ^{17}O-excess=–161 per meg[53]. The ^{17}O-excess of 0, –5 per meg[13], and –17 per meg (this study) of seawater with respect to VSMOW give temperature estimations of 12, 14, and 20 °C, respectively, based on Eq. (5). For comparison, the calculated temperature based on measured quartz-water fractionation factor $\alpha^{18}O_{quartz\text{-}water}$ is 17 °C in the original study[53].

5.2 OCEAN ISOTOPE MASS BALANCE MODEL

A classic ocean isotope mass balance model was constructed by Muehlenbachs and Clayton[60] which demonstrated that oxygen isotopic composition of ocean water has not changed in the phanerozoic. It was recently expanded to include $^{17}O/^{16}O$ ratio[61-62]. Oxygen isotopic compositions of seawater on a global scale are controlled by processes such as high-temperature alteration of oceanic crust, low-temperature alteration of oceanic crust, continental weathering, continental growth, and mantle recycling. Isotope-mass-balance

calculations by Sengupta and Pack[62] yielded a steady state after 2.6×10^8 years with $\delta^{18}O$=–0.36±0.5 ‰ and ^{17}O-excess=–17±12 per meg for a modern ice-free world. The $\delta^{18}O$ for modern world is about 1 ‰ more positive than that of the ice-free world[63], and the ^{17}O-excess for modern world is about 1 per meg more negative than that of the ice-free world[62]. In order to achieve ^{17}O-excess =–4 per meg for the modern ice-free world (^{17}O-excess = –5 per meg of the modern world, correspondingly), high-*T* ocean floor alteration flux would have to be lowered by 40 % or the continental weathering flux would have to be increased by 75 %, or a combination of 25 % lower high-*T* ocean floor alteration flux and 25 % higher continental weathering flux given by Muehlenbachs[64]. Thus, results from this study with ^{17}O-excess= –17±5 per meg support the ocean isotope mass balance model without quantitatively changing the major fluxes. While Sengupta and Pack[62] model used λ=0.5305, the ocean endmember recalculated with λ=0.528 is ^{17}O-excess=–18±12 per meg, again consistent with our observations.

5.3 RELEVANCE TO GROSS OXYGEN PRODUCTIVITY

Photosynthetic O_2 has an isotopic composition similar to the source water and tropospheric O_2 is anomalously depleted in ^{17}O due to O_3 and CO_2 photochemistry in the lower stratosphere. Mixed layer gross oxygen productivity (GOP) can be estimated by mass balance equation that account for relative contribution of these two end-members[65]. Observation of this natural tracer $^{17}\Delta$ of dissolved O_2 in the mixed layer to constrain marine productivity has been

throughout the global ocean[66]. The ratio of GOP to gross Air-O_2 invasion, *g*, is calculated by dual-delta method as Eq. (6)[67-69]:

$$g = \frac{(1+{}^{17}\varepsilon_E)\frac{{}^{17}\delta - {}^{17}\delta_{sat}}{1+{}^{17}\delta} - \gamma_R(1+{}^{18}\varepsilon_E)\frac{{}^{18}\delta - {}^{18}\delta_{sat}}{1+{}^{18}\delta} + s({}^{17}\varepsilon_E - \gamma_R {}^{18}\varepsilon_E)}{\frac{{}^{17}\delta_P - {}^{17}\delta}{1+{}^{17}\delta} - \gamma_R \frac{{}^{18}\delta_P - {}^{18}\delta}{1+{}^{18}\delta}} \quad (6)$$

where δ, δ_{sat}, δ_p refer to the δvalues of dissolved O_2, dissolved O_2 at air saturation, and photosynthetic O_2, respectively, with respect to Air-O_2, ε_E is kinetic fractionation in evasion from sea to air and *s* is relative supersaturation of dissolved O_2. The ${}^{18}\delta_{sat}$=0.707 ‰, ${}^{17}\delta_{sat}$=0.382 ‰, ${}^{17}\varepsilon_E$=–1.463 ‰, ${}^{18}\varepsilon_E$=–2.800 ‰. The γ_R=0.5179 characterizes respiratory fractionation. Photosynthetic process is characterized by small isotope fractionation from source water. Taking ${}^{18}\delta_W$=–23.647 ‰ and ${}^{17}\delta_W$=–12.107 ‰ of ocean water with respect to Air-O_2, accounted for the 5 per meg lower ${}^{17}O/{}^{16}O$ of ocean water compared to VSMOW, photosynthetic O_2 has ${}^{18}\delta_P$=–19.625 ‰ and ${}^{17}\delta_P$=–9.980 ‰, the average of a strain of cyanobacterium and four phytoplankton species[68]. Using a dataset of triple oxygen isotope measurements in the Southern Ocean[70], assuming $s=s_{bio}=\Delta(O_2/Ar)$ from the dataset, our calculation yielded similar results as Kaiser and Abe[68] (Figure 5). If accounting for the 17 per meg lower ${}^{17}O/{}^{16}O$ of ocean water compared to VSMOW from this study (taking as bulk ocean value), average ${}^{18}\delta_P$=–19.625 ‰ and ${}^{17}\delta_P$=–9.997 ‰ (the corresponding ${}^{17}O$-excess=218 per meg calculated at λ=0.5179 is closer to incubation experimental value of ~210

per meg[71]), *g* values are relatively smaller at the same $\delta^{18}O$ and the differences are more prominent at higher *g* values (Figure 5).

In the recent years, it is observed that the mixed layer has a component of ^{17}O-enriched O_2 accumulated in the less vented thermocline by either entrainment of water or vertical turbulent flux from the thermocline, which results in an overestimation of mixed layer GOP[72-78]. Wurgaft et al.[74] added a term for GOP contribution from beneath the mixed layer to a simplified form of Eq.(6). Haskell et al.[78] divided the euphotic regions into mixed layer and below-mixed-layer (BML) and constructed similar equations with GOP of the mixed layer influenced by the BML, and GOP of BML influenced by the deep water column below the euphotic depth. An implication of the results from this study is that deeper water may have a different isotopic composition as surface water, thus isotopic compositions of photosynthetic O_2 may differ in each layer, impacting the quantification of GOP in euphotic regions including mixed layer and BML.

Isotopic compositions of water endmember is crucial for accurate estimation of GOP and should be analyzed more prevalently by modern techniques such as laser spectroscopy.

5.4 RELEVANCE TO PALEO-HUMIDITY STUDIES

The ^{17}O-excess value of vapor and precipitation has been used as a unique quantitative tracer for the relative humidity in oceanic moisture source regions and thus a useful proxy for hydrology and paleoclimatology[10, 79-82]. Convection and

snow formation overprinting ^{17}O-excess signature from ocean source regions are reported for our complex nature[8, 9, 83].

In the example below, we estimate kinetic fractionation factor for the interfacial layer between sea surface and the atmosphere ($^{18}\alpha_{\text{diff}}$), from the correlation between ^{17}O-excess and relative humidity of modern ocean. The α_{diff} is applied to study paleo-humidity[11] and is an important parameter in evaporation models[79].

The ^{17}O-excess value of marine vapor is given by Eq. (7):

$$^{17}O - excess = -\ln\left[{}^{18}\alpha_{eq}^{0.529}\left({}^{18}\alpha_{diff}^{0.518}(1-h_n)+h_n\right)\right] + 0.528\ln\left[{}^{18}\alpha_{eq}\left({}^{18}\alpha_{diff}(1-h_n)+h_n\right]\right.$$

Eq. (7)

In Eq. (7), the ^{17}O-excess of marine vapor is defined with respect to ocean water, rather than VSMOW. Luz and Barkan[13] took ^{17}O-excess of ocean waters at 0-5390 m depth as ^{17}O-excess of bulk ocean water relative to VSMOW for this correction. Although our data mostly represent deep water, there's no significant depth variation and we cannot differentiate the λ value of Mariana Trench data from that of surface equilibrium or that of Luz and Barkan[13] at 95% confidence level. Therefore our data may represent bulk ocean isotopic composition and may also be suitable for studies of humidity at moisture source region.

In Eq. (7), the exponent θ_{eq}=0.529 is associated with equilibrium liquid water-water vapor fractionation and θ_{diff}=0.518 is associated with water vapor diffusion into air. At a sea surface temperature of 10 ^{o}C, the equilibrium fractionation factor $^{18}\alpha_{eq}$ equals 1.01073[40]. The $^{18}\alpha_{diff}$ is estimated by fitting the right side of Eq. (7) to the left side, measured ^{17}O-excess of marine vapor over the Southern Ocean[79]. Samples with h_n>80% are excluded for the same reasoning (giving less errors in $^{18}\alpha_{diff}$) as in the original study. Luz and Barkan[13] obtained a $^{18}\alpha_{diff}$=1.009 (RMSE=7.9 per meg) applying an average $^{17}O_{excess}$ of –5 per meg of seawater with respect to VSMOW to each ^{17}O-excess datum of marine vapor measured with respect to VSMOW. Taking the similar approach with the average $^{17}O_{excess}$=–17 per meg of Mariana Trench waters from this study, the best-fit value is $^{18}\alpha_{diff}$=1.0122 (RMSE=9 per meg) (Figure 6), in comparison to $^{18}\alpha_{diff}$=1.008 taking seawater as VSMOW[79], and $^{18}\alpha_{diff}$=1.005 based on wind tunnel experiments[84]. If we apply seawater $^{17}O_{excess}$=–14 per meg, with respect to VSMOW, from 12 samples at 5-3000 m depth in this study, $^{18}\alpha_{diff}$=1.0115 (RMSE=9 per meg).

The $^{18}\alpha_{diff}$ spans the whole range from 1 (pure turbulent transport) to 1.0319 (pure molecular diffusion)[35, 84, 85]. Kinetic fractionation factor $^{18}\alpha_{diff}$=1.014 of water vapor diffusion into air is commonly used for lake systems[86]. Our estimations of $^{18}\alpha_{diff}$ of 1.0122 and 1.0115 based on Southern Ocean marine vapor data reflect

differential contributions of turbulence and molecular diffusion. Those are choices to estimate paleo-humidity with ice cores[11].

6. CONCLUSIONS

Forty Mariana Trench water samples collected at 5-10923 m were analyzed at LSCE, France. λ=0.521 $\pm$ 0.003 (1σ) for Mariana Trench water samples is consistent with surface equilibrium isotope signals modified by kinetic processes in the ocean interior and sea-ice formation at the deep water source region: circum-Antarctica. The ^{17}O-excess=–17$\pm$5 per meg (1σ) from this new dataset is notably lower than that of the global database of Luz and Barkan[13], mostly from shallower depths at Eastern Pacific and Atlantic. The observation of ^{17}O-excess at Mariana Trench matches predicted ocean ^{17}O-excess value by ocean isotope mass balance model. Given the geographically constrained sampling in this study, the consistency between our observation and model prediction should be further tested and confirmed across deep ocean basins. Such an effort is justified because ocean water triple oxygen isotopic compositions are important for the application of triple oxygen isotope thermometry, quantification of gross oxygen productivity in euphotic regions and relative humidity in oceanic moisture source regions.

Author Contributions

The manuscript was written through contributions of all authors. All authors have given approval to the final version of the manuscript. Ying Lin, Nanping Wu, Kaiwen Ta, Amaelle Landais, Xiaotong Peng contributed equally.

Supporting Information: Additional equations, and tables including temperatures and salinities recorded by the CTD in sample collection.

ACKNOWLEDGMENT

The authors are grateful for the Deep-sea Institute of Science and Technology, Chinese Academy of Sciences for sample collection and the financial support for sample analyses (N.W., Grant no.E01X0301). The authors thank the Laboratory of Climate and Environmental Sciences (LSCE), France for sample analyses. The authors greatly appreciate extensive and constructive comments from reviewers. Y. Lin memorializes Robert N. Clayton for his mentorship and she is thankful to Marilyn Fogel for financial support.

References:

1. McKinney C.R., McCrea C.J., Epstein S., Allen H.A., Urey H.C., Improvements in mass spectrometers for the measurement of small differences in isotope abundance ratios. *The Review of scientific instruments* **21**, 724-730 (1950). DOI: 10.1063/1.1745698.

2. Matsuhisa Y., Goldsmith J.R., Clayton R.N., Mechanisms of hydrothermal crystallization of quartz at 250°C and 15 kbar. *Geochimica et Cosmochimica Acta* **42**, 173-182 (1978). DOI: 10.1016/0016-7037(78)90130-8.
3. Young E.D., Galy A., Nagahara H., Kinetic and equilibrium mass-dependent isotope fractionation laws in nature and their geochemical and cosmochemical significance. *Geochimica et Cosmochimica Acta* **66**, 1095-1104 (2002). DOI: 10.1016/S0016-7037(01)00832-8.
4. Herwartz D., Triple Oxygen Isotope Variations in Earth's Crust**.** *Reviews in Mineralogy and Geochemistry* **86**, 291–322 (2021). DOI: 10.2138/rmg.2021.86.09.
5. Barkan E., Luz B., High precision measurements of $^{17}O/^{16}O$ and $^{18}O/^{16}O$ ratios in H_2O. *Rapid Communications in Mass Spectrometry* **19**, 3737-3742 (2005). DOI: 10.1002/rcm.2250.
6. Barkan E., Luz B., Diffusivity fractionations of $H_2{}^{16}O/H_2{}^{17}O$ and $H_2{}^{16}O/H_2{}^{18}O$ in air and their implications for isotope hydrology. *Rapid Communications in Mass Spectrometry* **21**, 2999-3005 (2007). DOI:10.1002/rcm.3180.
7. Li S., Levin N.E., Chesson L.A., Continental scale variation in 17O-excess of meteoric waters in the United States. *Geochimica et Cosmochimica Acta* **164**, 110-126 (2015). DOI: 10.1016/j.gca.2015.04.047.
8. Schoenemann S.W., Steig E.J., Ding Q., Markle B.R., Schauer A.J., Triple water-isotopologue record from WAIS Divide, Antarctica: Controls on glacial-

436 interglacial changes in $^{17}O_{excess}$ of precipitation. *J. Geophys. Res. Atmos.* **119**, 8741– 8763 (2014). DOI:10.1002/2014JD021770.

438 9. Schoenemann S.W., Steig E.J., Seasonal and spatial variations of $^{17}O_{excess}$ and d_{excess} in Antarctic precipitation: Insights from an intermediate complexity isotope model. *J. Geophys. Res. Atmos.* **121**, 11,215–11,247 (2016). DOI:10.1002/2016JD025117.

442 10. Landais A., Steen-Larsen H.C., Guillevic M., Masson-Delmotte V., Vinther B., Winkler R., Triple isotopic composition of precipitation in surface snow and water vapor at NEEM (Greenland). *Geochimica et Cosmochimica Acta* **77**, 304-316 (2012). DOI:10.1016/j.gca.2011.11.022.

446 11. Winkler R., Landais A., Sodemann H., Dümbgen L., Prié F. et al., Deglaciation records of ^{17}O-excess in East Antarctica: reliable reconstruction of oceanic normalized relative humidity from coastal sites. *Climate of the Past* **8**, 1-16 (2012). DOI: 10.5194/cp-8-1-2012.

450 12. Meijer H.A.J., Li W.J., The use of electrolysis for accurate $\delta^{17}O$ and $\delta^{18}O$ isotope measurements in water. *Isotopes in Environmental and Health Studies* **34**, 349-369 (1998). DOI: 10.1080/10256019808234072.

453 13. Luz B., Barkan E., Variations of $^{17}O/^{16}O$ and $^{18}O/^{16}O$ in meteoric waters. *Geochimica et Cosmochimica Acta* **74**, 6276-6286 (2010). DOI:10.1016/j.gca.2010.08.016.

14. Chacko T., Cole D.R., Horita J., Equilibrium oxygen, hydrogen and carbon isotope fractionation factors applicable to geologic systems. *Reviews in Mineralogy and Geochemistry* **43**, 1-81 (2001). DOI: 10.2138/gsrmg.43.1.1.
15. Lisiecki L.E., Raymo M.E., A Pliocene-Pleistocene stack of 57 globally distributed benthic $\delta^{18}O$ records. *Paleoceanography* **20**, PA1003 (2005). DOI: 10.1029/2004PA001071.
16. Railsback L.B., Gibbard P.L., Head M.J., Voarintsoa N.R.G., Toucanne S., An optimized scheme of lettered marine isotope substages for the last 1.0 million years, and the climatostratigraphic nature of isotope stages and substages. *Quaternary Science Reviews* **111**, 94-106 (2015). DOI: 10.1016/j.quascirev.2015.01.012.
17. Vho A., Lanari P., Rubatto D., An internally-consistent database for oxygen isotope fractionation between minerals. *Journal of Petrology* **60**, 2101-2130 (2019). DOI: 10.1093/petrology/egaa001.
18. Cao X., Bao H., Redefining the utility of the three-isotope method. *Geochimica et Cosmochimica Acta **212***, 16-32 (2017). DOI: 10.1016/j.gca.2017.05.028.
19. Guo W.**,** Zhou C., Triple oxygen isotope fractionation in the DIC-H_2O-CO_2 system: A numerical framework and its implications. *Geochim. Cosmochim. Acta*. **246**, 541-564 (2019). DOI: 10.1016/j.gca.2018.11.018.
20. Herwartz D., Pack A., Krylov D., Xiao Y., Muehlenbachs K., Sengupta S., Rocco T.D., Revealing the climate of snowball Earth. *Proceedings of the*

National Academy of Sciences **112**, 5337-5341 (2015). DOI: 10.1073/pnas.1422887112.

21. Levin N.E., Raub T.D., Dauphas N., Eiler J.M., Triple oxygen isotope variations in sedimentary rocks. *Geochimica et Cosmochimica Acta* **139**, 173-189 (2014). DOI: 10.1016/j.gca.2014.04.034.
22. Wostbrock J.A.G., Sharp Z.D., Triple oxygen isotopes in silica–water and carbonate–water systems. *Reviews in Mineralogy and Geochemistry* **86**, 367-400 (2021). DOI: 10.2138/rmg.2021.86.11.
23. Sengupta S., Peters S.T.M., Reitner J., Duda J.-P., Pack A., Triple oxygen isotopes of cherts through time. *Chemical Geology* **554**, 119789 (2020). DOI; 10.1016/j.chemgeo.2020.119789.
24. Aron P.G., Levin N.E., Beverly E.J., Huth T.E., Passey B.H., Pelletier E.M., Poulsen C.J., Winkelstern I.Z., Yarian D.A., Triple oxygen isotopes in the water cycle, *Chemical Geology* **565**, 120026 (2021). DOI: 10.1016/j.chemgeo.2020.120026.
25. Bigg G.R., Rohling E.J., An oxygen isotope data set for marine waters. *Journal of Geophysical Research: Oceans* **105**, 8527-8535 (2000). DOI: 10.1029/2000JC900005.
26. The Nansen Legacy. Sampling Protocols: Version 7. The Nansen Legacy Report Series 17/2021. DOI: https://doi.org/10.7557/nlrs.5793.
27. Landais A., Winkler R., Prié F., Triple isotopic composition of oxygen in water from ice cores. Thermo Scientific Application Note 30287 (2014).

28. Schoenemann S.W., Schauer A.J., Steig E.J., Measurement of SLAP2 and GISP $\delta^{17}O$ and proposed VSMOW-SLAP normalization for $\delta^{17}O$ and $^{17}O_{excess}$. *Rapid Communications in Mass Spectrometry* **27**, 582–590 (2013). DOI: 10.1002/rcm.6486.

29. Schmidt G.A., Bigg G.R., Rohling E.J., *Global Seawater Oxygen-18 Database - v1.22 https://data.giss.nasa.gov/o18data/* (1999).

30. LeGrande A.N., Schmidt G.A., Global gridded data set of the oxygen isotopic composition in seawater. *Geophysical Research Letters* **33**, L12604 (2006). DOI: 10.1029/2006GL026011.

31. Yeung L.Y., Hayes J.A., Climbing to the top of mount Fuji: Uniting theory and observations of oxygen triple isotope systematics. *Reviews in Mineralogy and Geochemistry* **86**, 97-135 (2021). DOI: 10.2138/rmg.2021.86.03**.**

32. Wostbrock J.A.G., Cano E.J., Sharp Z.D., An internally consistent triple oxygen isotope calibration of standards for silicates, carbonates and air relative to VSMOW2 and SLAP2. *Chemical Geology* **533**, 119432 (2020). DOI:10.1016/j.chemgeo.2019.119432.

33. Sharp Z.D., *Principles of Stable Isotope Geochemistry*, 2nd Edition (2017). DOI:10.25844/h9q1-0p82.

34. Craig H., Gordon L.I., Deuterium and oxygen 18 variations in the ocean and the marine atmosphere in *Stable Isotopes in Oceanographic Studies and Paleotemperatures*, E. Tongiorgi, Ed. (Pisa : V. Lischi, 1965). pp.121-130.

35. Horita J., Rozanski K., Cohen S., Isotope effects in the evaporation of water: a status report of the Craig–Gordon model. *Isotopes in Environmental and Health Studies* **44**, 23-49 (2008). DOI: 10.1080/10256010801887174.

36. Gonfiantini R., Wassenaar L.I., Araguas-Araguas L., Aggarwal P.K., A unified Craig-Gordon isotope model of stable hydrogen and oxygen isotope fractionation during fresh or saltwater evaporation. *Geochimica et Cosmochimica Acta* **235**, 224-236 (2018). DOI: 10.1016/j.gca.2018.05.020.

37. Gonfiantini R., Wassenaar L.I., Araguas-Araguas L.J., Stable isotope fractionations in the evaporation of water: The wind effect. *Hydrological Processes* **34**, 3596-3607 (2020). DOI: 10.1002/hyp.13804.

38. Cao X., Liu Y., Equilibrium mass-dependent fractionation relationships for triple oxygen isotopes. *Geochimica et Cosmochimica Acta* **75**, 7435-7445 (2011). DOI: 10.1016/j.gca.2011.09.048.

39. Angert A., Cappa C.D., DePaolo D.J., Kinetic ^{17}O effects in the hydrologic cycle: Indirect evidence and implications. *Geochimica et Cosmochimica Acta* **68**, 3487-3495 (2004). DOI: 10.1016/j.gca.2004.02.010.

40. Horita J., Wesolowski D.J., Liquid-vapor fractionation of oxygen and hydrogen isotopes of water from the freezing to the critical temperature. *Geochimica et Cosmochimica Acta* **58**, 3425-3437 (1994), DOI: 10.1016/0016-7037(94)90096-5.

41. MacKinnon J., Mountain waves in the deep ocean. *Nature* **501,** 321–322 (2013). DOI: 10.1038/501321a.

42. Griffies S.M., Winton M., Anderson W.G., Benson R., Delworth T.L. et al., Impacts on Ocean Heat from Transient Mesoscale Eddies in a Hierarchy of Climate Model. *Journal of Climate* **28**: 952–977 (2014). DOI: 10.1175/JCLI-D-14-00353.1.
43. Fontes J.C., Letolle R., Marcé A., Some results of oxygen isotope studies of marine waters in *Stable Isotopes in Oceanographic Studies and Paleotemperatures*, E. Tongiorgi, Ed. (Pisa : V. Lischi, 1965). pp. 131-141.
44. Richardson J.L., Bergsteinsson P., Getz R.J., Peters D.L., Sprague R.W., "Sea Water Mass Diffusion Coefficient Studies" PHILCO Publication No. U-3021 (1965).
45. Harris K.R., Woolf L.A., Pressure and temperature dependence of the self diffusion coefficient of water and oxygen-18 water. *Journal of the Chemical Society, Faraday Transactions 1: Physical Chemistry in Condensed Phases* **76,** 377-385 (1980). DOI: 10.1039/F19807600377.
46. Chapman S., Cowling T.G., *The mathematical theory of non-uniform gases: An account of the kinetic theory of viscosity, Thermal Conduction and Diffusion in Gases*, D. Burnett, Ed. (Cambridge University Press, 1990).
47. Hopp M., Mele J., Gross J., Self-diffusion coefficients from entropy scaling using the PCP-SAFT equation of state. *Industrial & Engineering Chemistry Research* **57**, 12942-12950 (2018). DOI: 10.1021/acs.iecr.8b02406.
48. Lohmann R., Jurado E., Dijkstra H.A., Dachs J., Vertical eddy diffusion as a key mechanism for removing perfluorooctanoic acid (PFOA) from the global

surface oceans. *Environmental Pollution* **179**, 88-94 (2013). DOI: 10.1016/j.envpol.2013.04.006.

49. Clayton R.N., Mayeda T.K., Kinetic isotope effects in oxygen in the laboratory dehydration of magnesian minerals. *The Journal of Physical Chemistry A* **113**, 2212-2217 (2009). DOI: 10.1021/jp808621n.
50. Sarmiento J.L., Gruber N., Ocean Biogeochemical Dynamics. Princeton, Woodstock: Princeton University Press (2006). pp.528.
51. Souchez R., Jouzel J., Lorrain R., Sleewaegen S., Stiévenard M., Verbeke V., A kinetic isotope effect during ice formation by water freezing. *Geophysical Research Letters* **27**, 1923-1926, DOI: 10.1029/2000GL006103.
52. Sharp Z.D., Wostbrock J.A.G., Pack A., Mass-dependent triple oxygen isotope variations in terrestrial materials. *Geochem. Persp. Let.* **7**, 27–31 (2018). DOI: 10.7185/geochemlet.1815.
53. Sharp Z.D., Gibbons J.A., Maltsev O., Atudorei V., Pack A. *et al.*, A calibration of the triple oxygen isotope fractionation in the SiO_2–H_2O system and applications to natural samples. *Geochimica et Cosmochimica Acta* **186**, 105-119 (2016). DOI: 10.1016/j.gca.2016.04.047.
54. Wostbrock J.A.G., Brand U., Coplen T.B., Swart R.K., Carlson S.J. *et al.*, Calibration of carbonate-water triple oxygen isotope fractionation: Seeing through diagenesis in ancient carbonates. *Geochimica et Cosmochimica Acta* **288**, 369-388 (2020). DOI: 10.1016/j.gca.2020.07.045.

55. Hayles J.A., Cao X., Bao H., The statistical mechanical basis of the triple isotope fractionation relationship. *Geochemical Perspectives Letters* **3**, 1-11 (2016) DOI: 10.7185/geochemlet.1701.

56. Hayles J.A, Gao C., Cao X., Liu Y., Bao H., Theoretical calibration of the triple oxygen isotope thermometer. *Geochimica et Cosmochimica Acta* **235**, 237-245 (2018). DOI: 10.1016/j.gca.2018.05.032.

57. Schauble E.A., Young E.D., Mass dependence of equilibrium oxygen isotope fractionation in carbonate, nitrate, oxide, perchlorate, phosphate, silicate, and sulfate minerals. *Reviews in Mineralogy and Geochemistry* **86**, 137-178 (2021). DOI: 10.2138/rmg.2021.86.04.

58. Gibbons J., Calibration and application of a silica-water single mineral thermometer to geothermal systems in Iceland and Chile. (University of New Mexico thesis, 2016).

59. Wostbrock J.A.G., Sharp Z.D., Sanchez-Yanez C., Reich M., van den Heuvel D.B. *et al.*, Calibration and application of silica-water triple oxygen isotope thermometry to geothermal systems in Iceland and Chile. *Geochimica et Cosmochimica Acta* **234**, 84-97 (2018). DOI: 10.1016/j.gca.2018.05.007.

60. Muehlenbachs K., Clayton R.N., Oxygen isotope composition of the oceanic crust and its bearing on seawater. *Journal of Geophysical Research* **81**, 4365-4369 (1976). DOI: 10.1029/JB081i023p04365.

61. Pack A., Herwartz D., The triple oxygen isotope composition of the Earth mantle and understanding $\Delta^{17}O$ variations in terrestrial rocks and minerals.

Earth and Planetary Science Letters **390**, 138-145 (2014). DOI:10.1016/j.epsl.2014.01.017.

62. Sengupta S., Pack A., Triple oxygen isotope mass balance for the Earth's oceans with application to Archean cherts. *Chemical Geology* **495**, 18-26 (2018). DOI:10.1016/j.chemgeo.2018.07.012.
63. Shackleton N., Kennett J., Paleotemperature History of the Cenozoic and the Initiation of Antarctic Glaciation: Oxygen and Carbon Isotope Analyses in DSDP Sites 277, 279 and 281. Deep Sea Drilling Project Initial Reports Volume 29 (1975). DOI:10.2973/DSDP.PROC.29.117.1975.
64. Muehlenbachs K., The oxygen isotopic composition of the oceans, sediments and the seafloor. *Chemical Geology* **145**, 263-273 (1998). DOI:10.1016/S0009-2541(97)00147-2.
65. Luz B., Barkan E., The isotopic ratios $^{17}O/^{16}O$ and $^{18}O/^{16}O$ in molecular oxygen and their significance in biogeochemistry. *Geochimica et Cosmochimica Acta* **69**, 1099-1110 (2005). DOI: 10.1016/j.gca.2004.09.001.
66. Juranek L.W., Quay P.D., Using Triple Isotopes of Dissolved Oxygen to Evaluate Global Marine Productivity. *Annual Review of Marine Science* **5**, 503-524 (2013). DOI: 10.1146/annurev-marine-121211-172430.
67. Kaiser J., Technical note: Consistent calculation of aquatic gross production from oxygen triple isotope measurements. *Biogeosciences* **8**, 1793–1811 (2011). DOI:10.5194/bg-8-1793-2011.

68. Kaiser J., Abe O., Reply to Nicholson's comment on "Consistent calculation of aquatic gross production from oxygen triple isotope measurements" by Kaiser (2011). *Biogeosciences* **9**, 2921–2933 (2012). DOI:10.5194/bg-9-2921-2012.

69. Prokopenko M.G., Pauluis O.M., Granger J., Yeung L.Y., Exact evaluation of gross photosynthetic production from the oxygen triple-isotope composition of O_2: Implications for the net-to-gross primary production ratios. *Geophys. Res. Lett.* **38**, L14603 (2011). DOI:10.1029/2011gl047652.

70. Reuer M.K., Barnett B.A., Bender M.L, Falkowski P.G., Hendricks M.B., New estimates of Southern Ocean biological production rates from O_2/Ar ratios and the triple isotope composition of O_2. *Deep Sea Research Part I: Oceanographic Research Papers* **54**, 951-974 (2007). DOI:10.1016/j.dsr.2007.02.007.

71. Manning C.C., Howard E.M., Nicholson D.P., Ji B.Y., Sandwith Z.O., Stanley R.H.R., Revising estimates of aquatic gross oxygen production by the triple oxygen isotope method to incorporate the local isotopic composition of water. *Geophysical Research Letters* **44**, 10,511– 10,519 (2017). DOI:10.1002/2017GL074375.

72. Nicholson D.P., Stanley R.H.R., Barkan E., Karl D.M., Luz B., Quay P.D., Doney S.C., Evaluating triple oxygen isotope estimates of gross primary production at the Hawaii Ocean Time-series and Bermuda Atlantic Time-series Study sites. *J. Geophys. Res.* **117**, C05012 (2012). DOI:10.1029/2010JC006856.

73. Nicholson D.P., Stanley R.H.R., Doney S.C., The triple oxygen isotope tracer of primary production in a dynamic ocean model. *Global Biogeochem. Cycles*, **28**, 538–552 (2014). DOI:10.1002/2013GB004704.

74. Wurgaft E., Shamir O., Angert A., Technical Note: The effect of vertical turbulent mixing on gross O_2 production assessments by the triple isotopic composition of dissolved O_2, *Biogeosciences Discuss.* **10**, 14,239–14,259 (2013). DOI:10.5194/bgd-10-14239-2013.

75. Jonsson B.F., Doney S.C., Dunne J., Bender M., Evaluation of Southern Ocean O_2/Ar based NCP estimates in a model framework. *Journal of Geophysical Research: Biogeosciences* **118**, 385–399 (2013). DOI:10.1002/jgrg.20032.

76. Castro-Morales K., Kaiser J., Using dissolved oxygen concentrations to determine mixed layer depths in the Bellingshausen Sea. *Ocean Sci.* **8**, 1–10 (2012). DOI: 10.5194/os-8-1-2012.

77. Howard E.M., Durkin C.A., Hennon G.M.M., Ribalet F., Stanley R.H.R., Biological production, export efficiency, and phytoplankton communities across 8000 km of the South Atlantic. *Global Biogeochem. Cycles* **31**, 1066–1088 (2017). DOI:10.1002/2016GB005488.

78. Haskell W.Z., Prokopenko M.G., Hammond D.E., Stanley R.H.R., Sandwith Z. O., Annual cyclicity in export efficiency in the inner Southern California Bight. *Global Biogeochem. Cycles* **31**, 357–376 (2017). DOI:10.1002/2016GB005561.

79. Uemura R., Barkan E., Abe O., Luz B., Triple isotope composition of oxygen in atmospheric water vapor. *Geophysical Research Letters* **37**, L04402 (2010). DOI: 10.1029/2009GL041960.

80. Landais A., Capron E., Toucanne S., Rhodes R., Popp T. et al., Ice core evidence for decoupling between midlatitude atmospheric water cycle and Greenland temperature during the last deglaciation. *Clim Past* **14**, 1405-1415. DOI: 10.5194/CP-14-1405-2018.

81. Uechi Y., Uemura R., Dominant influence of the humidity in the moisture source region on the ^{17}O-excess in precipitation on a subtropical island. *Earth and Planetary Science Letters* **513**, 20-28 (2019). DOI: 10.1016/j.epsl.2019.02.012.

82. Surma J., Assonov S., Staubwasser M., Triple oxygen isotope systematics in the hydrologic cycle. *Reviews in Mineralogy and Geochemistry* **86**, 401-428 (2021). DOI: 10.1515/9781501524677-013.

83. He S., Jackisc D., Samanta D., Kho P.Y.Y., Liu G., Wang X., Goodkin N.F., Understanding tropical convection through triple oxygen isotopes of precipitation from the Maritime Continent. *Journal of Geophysical Research: Atmospheres* **126**, e2020JD033418 (2021). DOI: 10.1029/2020JD033418.

84. Merlivat L., Jouzel J., Global climatic interpretation of the deuterium-oxygen 18 relationship for precipitation. *Journal of Geophysical Research* **84**, 5029-5033 (1979). DOI: 10.1029/JC084iC08p05029.

85. Cappa C.D., Hendricks M.B., DePaolo D.J., Cohen R.C., Isotopic fractionation of water during evaporation. *J. Geophys. Res.* 1**08**, 4525 (2003). DOI:10.1029/2003JD003597, D16.

86. Passey B.H., Ji H., Triple oxygen isotope signatures of evaporation in lake waters and carbonates: A case study from the western United States. *Earth and Planetary Science Letters* **518**, 1-12 (2019). DOI:10.1016/j.epsl.2019.04.026.

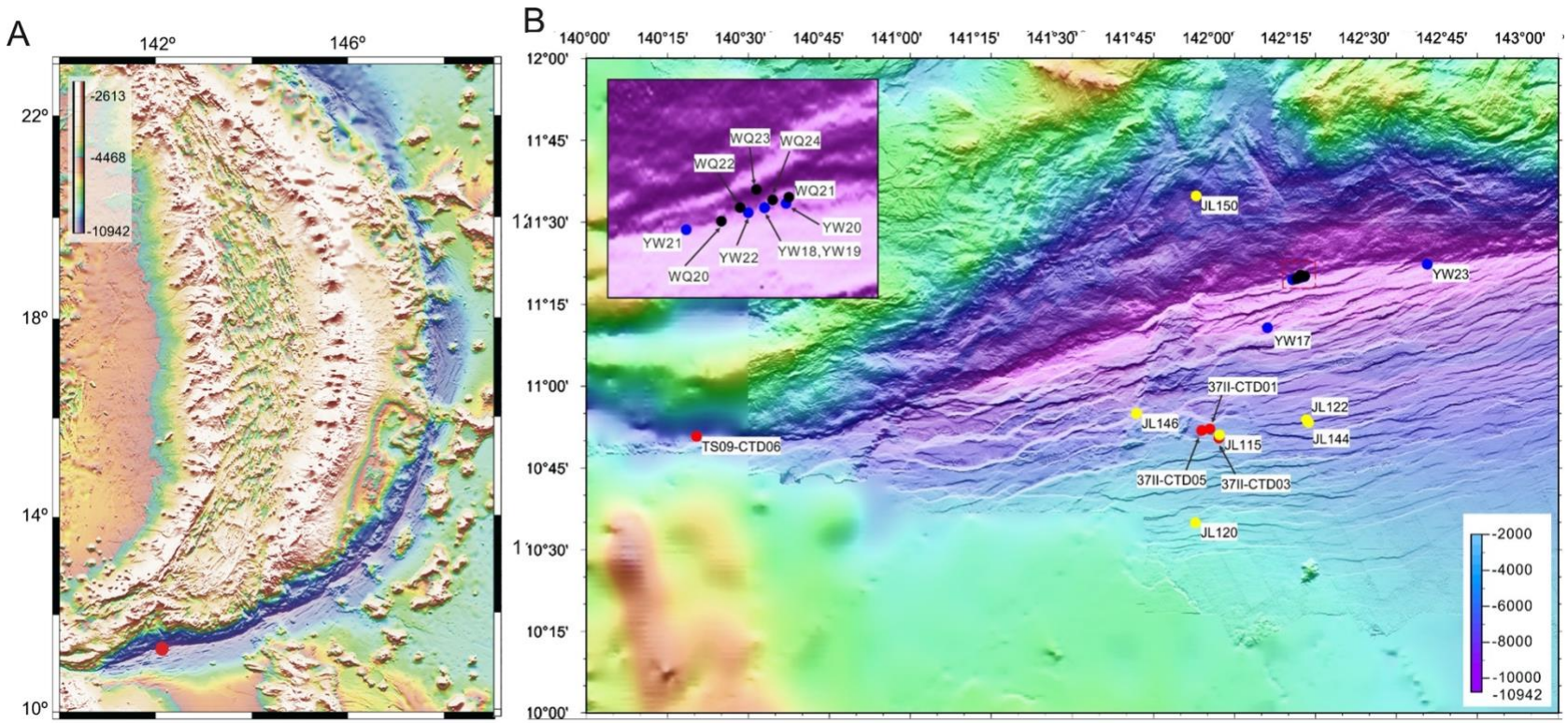

Figure 1. Bathymetry map and location of the sampling sites at the Mariana Trench. Red dot in A represents sampling site that is further detailed in B.

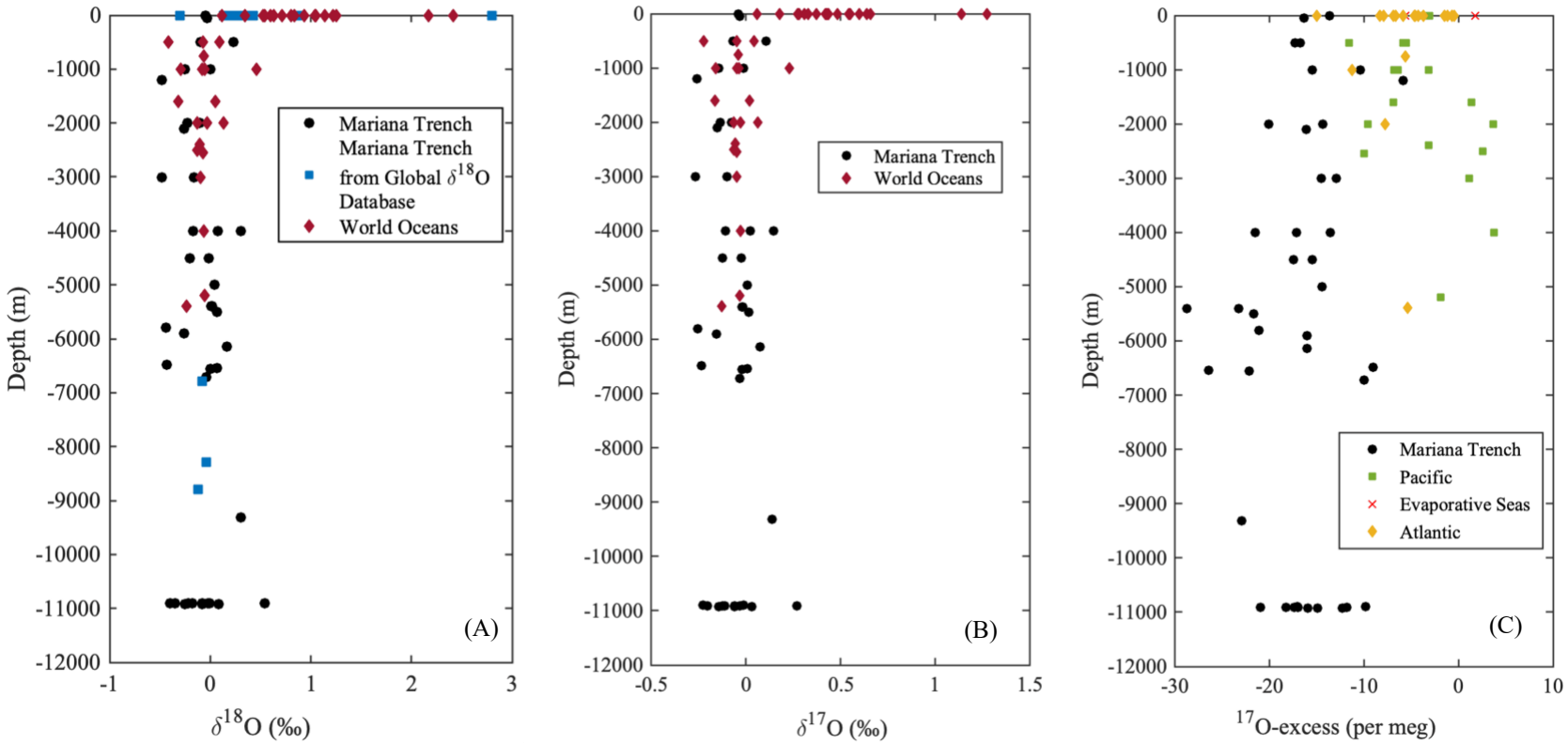

Figure 2. Depth profiles of seawater δ^{18}O (A), δ^{17}O (B), ^{17}O-excess (C) at Mariana Trench in this study, plotted with data from Global Seawater Oxygen-18 Database records at Mariana Trench[29] (reproduced from Schmidt G.A., Bigg G.R., Rohling E.J., 1999, "Global Seawater Oxygen-18 Database - v1.22", https://data.giss.nasa.gov/o18data/), and data from world oceans in Luz and Barkan[13].

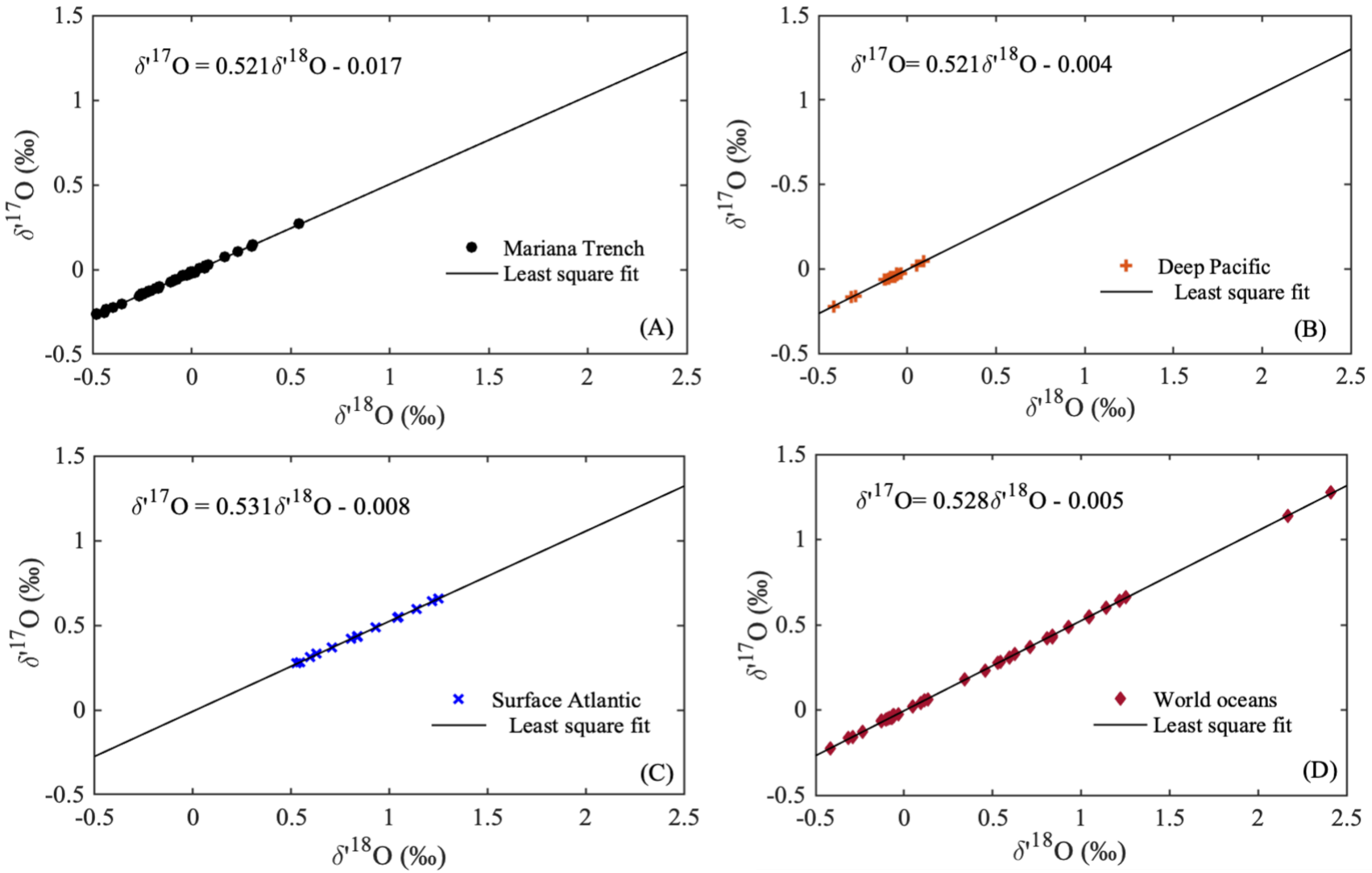

Figure 3. Oxygen three-isotope-plots of Mariana Trench waters from this study (A), deep Pacific (B), surface Atlantic (C), world oceans (D) from Luz and Barkan[13]. $\delta'^{x}O = 1000\ln(\delta^{x}O/1000+1)$, where *x* is 17 or 18.

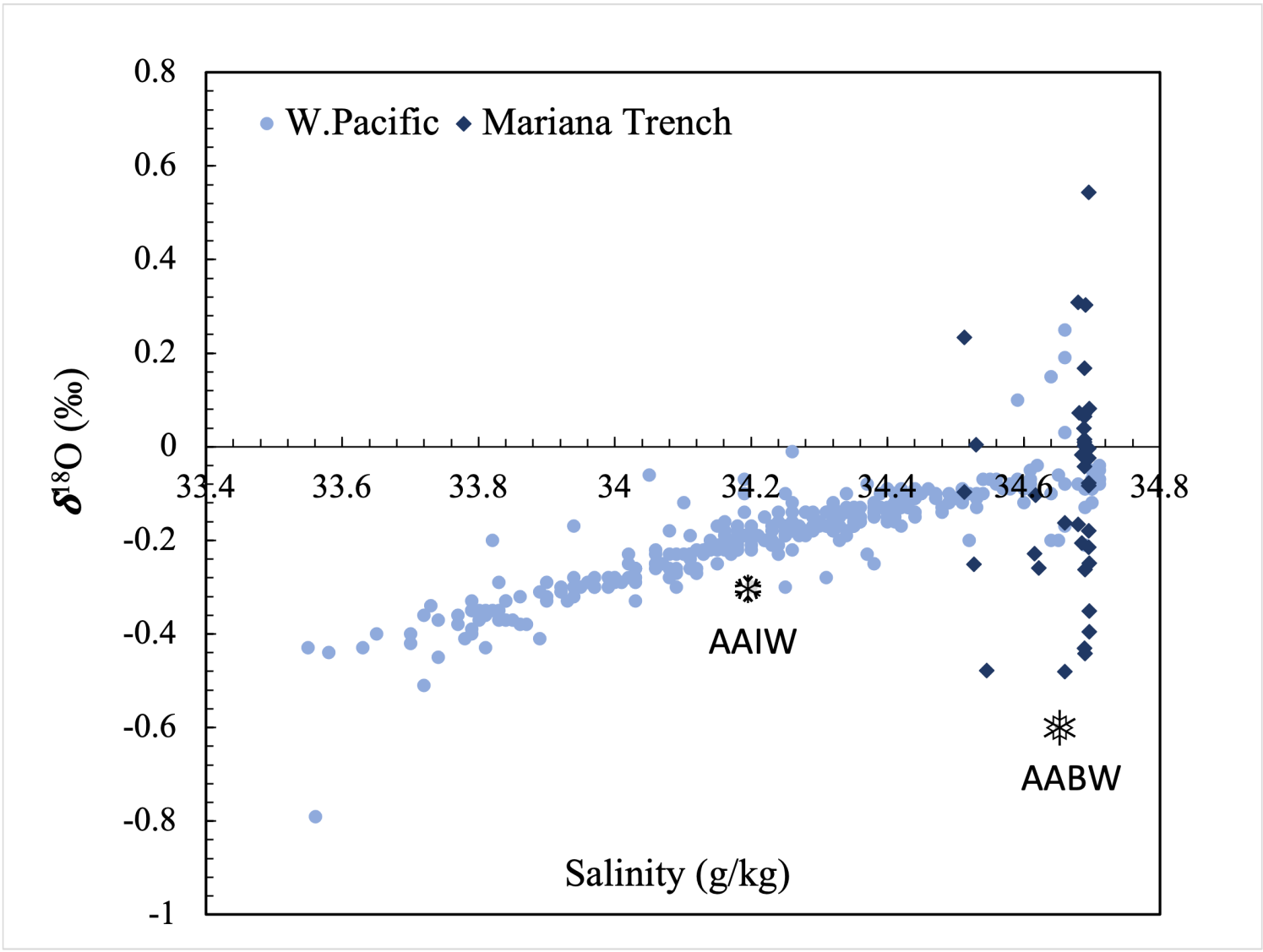

Figure 4. Correlation of $\delta^{18}O$ and salinity for water samples deeper than 500 m indicating mixing of AABW and AAIW to Pacific water body. W. Pacific data are from Global Seawater Oxygen-18 Database[29] (reproduced from Schmidt G.A., Bigg G.R., Rohling E.J., 1999, "Global Seawater Oxygen-18 Database - v1.22", https://data.giss.nasa.gov/o18data/).

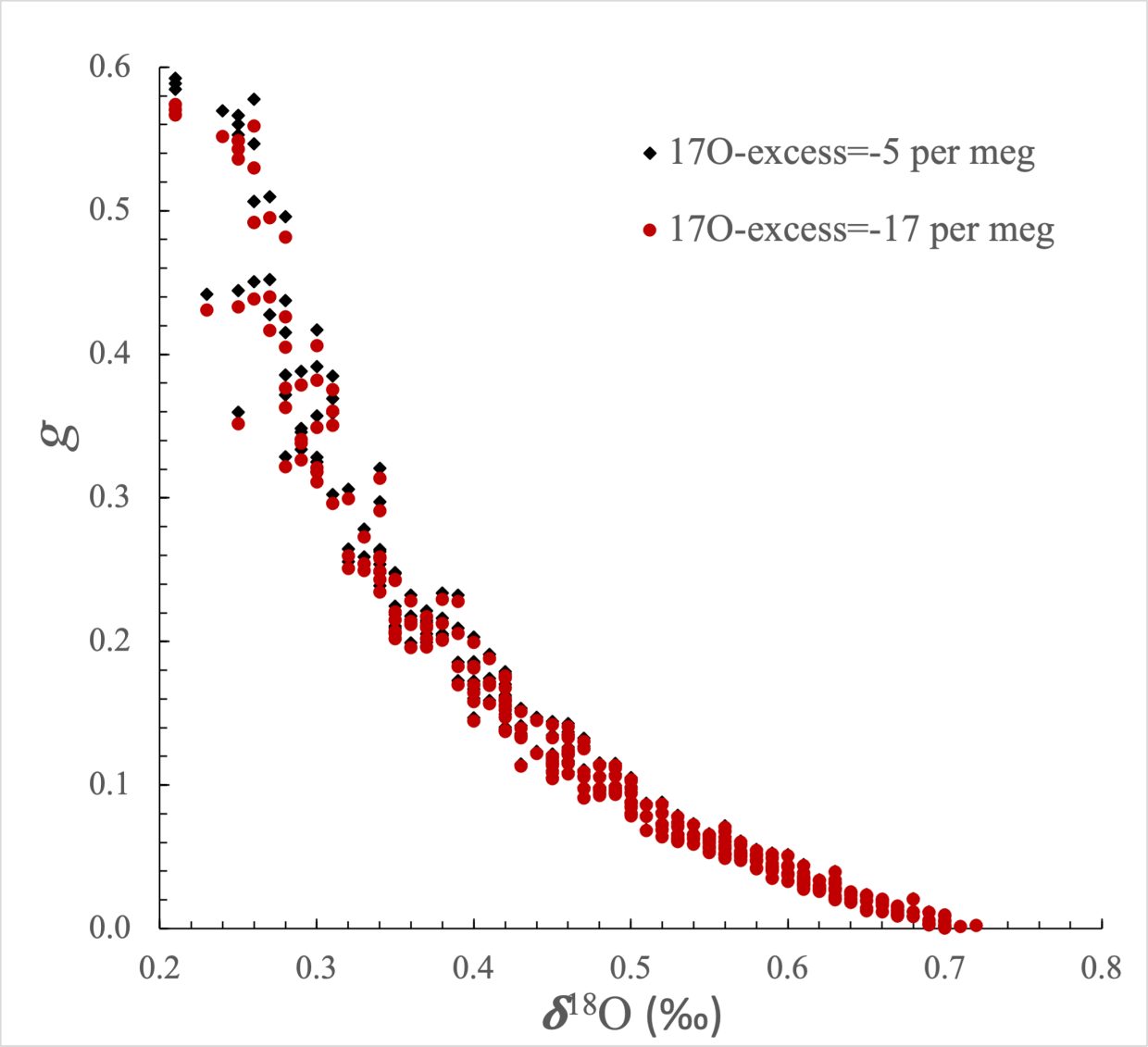

Figure 5. Gross oxygen productivity (GOP), *g*, estimated with ^{17}O-excess of seawater at –5 per meg[13] and –17 per meg (this study) with respect to VSMOW, using a Southern ocean dataset[70].

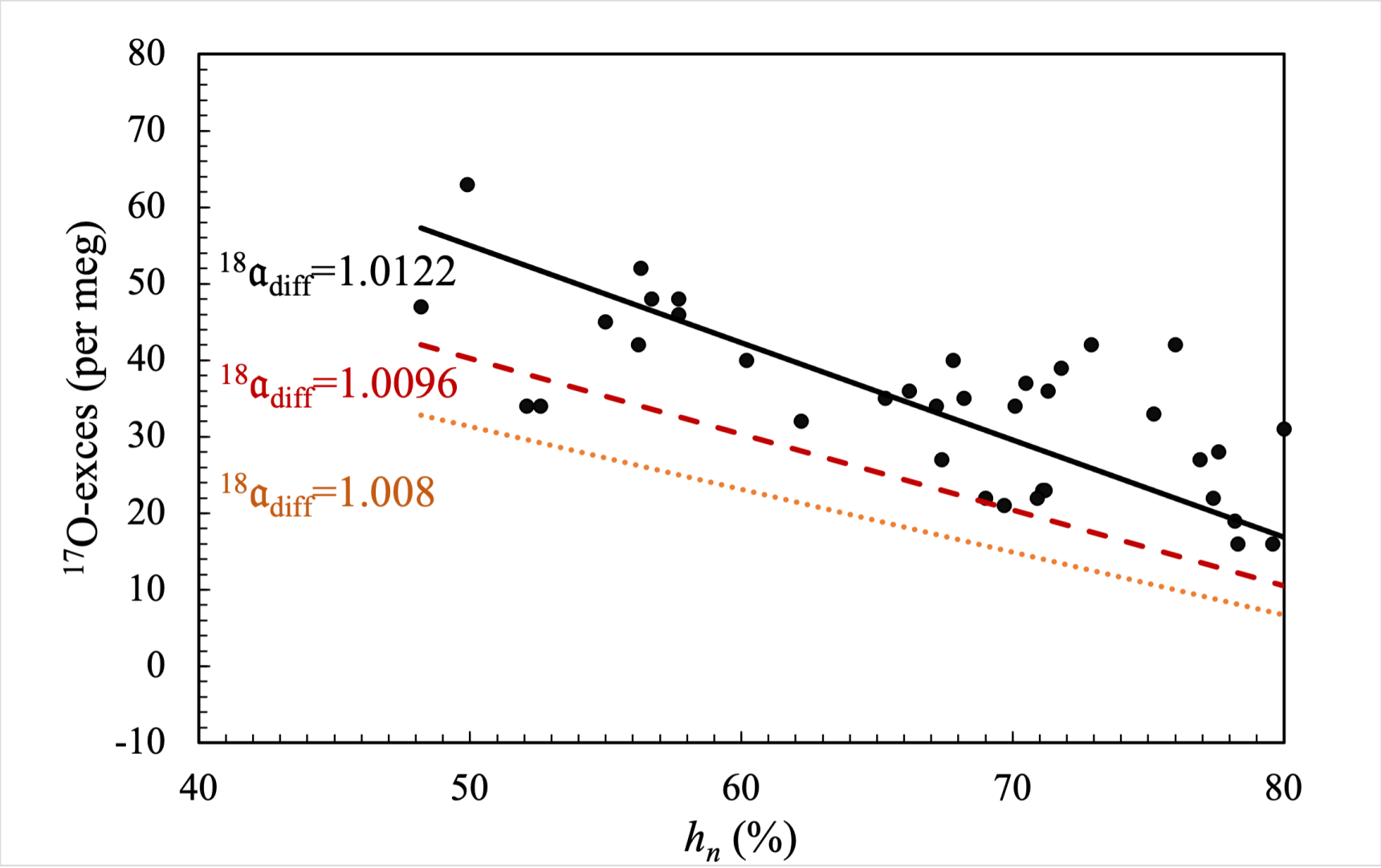

Figure 6. The best fit to Uemura et al.[79] is a model line based on Eq.(8) with $^{18}\alpha_{diff}$=1.0122, if seawater have ^{17}O-excess=–17 per meg with respective to VSMOW. $^{18}\alpha_{diff}$=1.0096 (maroon dashed line) for seawater having ^{17}O-excess=–5 per meg with respective to VSMOW[13], and 1.008 for seawater (orange dot line) having ^{17}O-excess=0 with respect to VSMOW[79].

Table 1. Triple oxygen isotopic compositions of Mariana Trench water samples.

Sample	Latitude (N)	Longitude (E)	Depth (m)	$\delta^{18}O$ (‰)	$\delta^{17}O$ (‰)	^{17}O-excess (per meg)
37II-CTD05-5m	10°51.875′	141°53.963′	5	–0.049	–0.040	–14
37II-CTD05-1000m	10°51.875′	141°53.963′	1000	0.005	–0.013	–15
37II-CTD05-2000m	10°51.875′	141°53.963′	2000	–0.104	–0.075	–20
37II-CTD05-3000m	10°51.875′	141°53.963′	3000	–0.480	–0.267	–13
37II-CTD05-4000m	10°51.875′	141°53.963′	4000	0.072	0.024	–14
37II-CTD05-5000m	10°51.875′	141°53.963′	5000	0.039	0.006	–14
37II-CTD05-5900m	10°51.875′	141°53.963′	5900	–0.263	–0.155	–16
37II-CTD01-50m	10°52.178′	141°55.451′	50	–0.028	–0.031	–16
37II-CTD01-500m	10°52.178′	141°55.451′	500	0.234	0.106	–17
37II-CTD01-1000m	10°52.178′	141°55.451′	1000	–0.251	–0.143	–10
37II-CTD01-2000m	10°52.178′	141°55.451′	2000	–0.229	–0.135	–14
37II-CTD01-4000m	10°52.178′	141°55.451′	4000	–0.166	–0.109	–22
37II-CTD03-1200m	10°50.480′	141°57.101′	1200	–0.478	–0.258	–6
37II-CTD03-2100m	10°50.480′	141°57.101′	2100	–0.260	–0.153	–16
37II-CTD03-3000m	10°50.480′	141°57.101′	3000	–0.163	–0.100	–14
37II-CTD03-4000m	10°50.480′	141°57.101′	4000	0.309	0.146	–17
37II-CTD03-4500m	10°50.480′	141°57.101′	4500	–0.206	–0.124	–16
37II-CTD03-5400m	10°50.480′	141°57.101′	5400	0.010	–0.018	–23
JL115	10.85097°	141.9537°	5497	0.071	0.016	–22

JL120	10.5824°	141.8796°	6717	–0.043	–0.032	–10
JL122	10.8976°	142.2218°	6140	0.168	0.073	–16
JL144	10.8889°	142.2289°	6560	0.002	–0.021	–22
JL146	10.9166°	141.6984°	6539	0.065	0.008	–26
JL150	11° 34.850'	141°52.930'	6479	–0.431	–0.237	–9
Dive-YW17	11°10.7160′	142°06.1020′	9320	0.303	0.137	–23
Dive-YW18	11°19.9844′	142°12.4887′	10910	–0.024	–0.034	–21
Dive-YW19	11°19.9844′	142°12.4887′	10901	–0.395	–0.226	–17
Dive-YW20	11°20.0742′	142°12.9313′	10912	–0.077	–0.059	–18
Dive-YW21	11°19.5011′	142°10.7433′	10902	–0.004	–0.012	–10
Dive-YW22	11°19.8720′	142°12.0900′	10920	0.082	0.031	–12
Dive-YW23	11°22.3440′	142°35.7284′	10922	–0.083	–0.060	–16
Dive-WQ20	11°19.6882′	142°11.5436′	10910	–0.215	–0.125	–12
Dive-WQ21	11°20.211′	142°13.034′	10910	–0.180	–0.112	–17
Dive-WQ22	11°19.9865′	142°11.9294′	10908	0.544	0.270	–17
Dive-WQ23	11°20.3824′	142°12.3219′	10910	–0.351	–0.202	–17
Dive-WQ24	11°20.1566′	142°12.6868′	10923	–0.249	–0.146	–15
TS09-CTD06-500m	10°50.7840′	140°20.400′	500	–0.097	–0.068	–17
TS09-CTD06-4500m	10°50.7840′	140°20.400′	4500	–0.018	–0.027	–17
TS09-CTD06-5400m	10°50.7840′	140°20.400′	5400	0.016	–0.020	–29
TS09-CTD06-5800m	10°50.7840′	140°20.400′	5800	–0.443	–0.255	–21

Table 2. Measurement standards at LSCE.

	$\delta^{18}O$ (‰) rel. VSMOW2	$\delta^{17}O$ (‰) rel. VSMOW2	^{17}O-excess (per meg) rel. VSMOW2	$\delta^{18}O$ (‰) VSMOW2/SLAP2 norm.	$\delta^{17}O$ (‰) VSMOW2/SLAP2 norm.	^{17}O-excess (per meg) VSMOW2/SLAP2 norm.
EPB8	–7.383	–3.89	15	–7.45	–3.926	15
HAWAI-1	0.516	0.272	0	0.521	0.275	0
VSMOW2	0	0	0	0	0	0
SLAP2	–55.001	–29.426	2	–55.5	–29.6989	0